Effect of dampers on the seismic performance of masonry walls assessed through fragility and demand hazard curves

Linda Giresini

Department of Civil and Industrial Engineering, University of Rome La Sapienza

linda.giresini@unipi.it

Abstract

In a damage avoidance design perspective, seismic rocking of rigid-like blocks, such as masonry walls, precast r.c./timber panels, art objects, etc., can be controlled through viscous elastic dampers. This paper discusses how to perform a seismic risk assessment of masonry walls undamped and damped by viscous-elastic dampers installed at the top of them. Firstly, a deterministic analysis allows understanding the role of the damper, whose coupling with a recentering component attenuates the motion, increases the rotation frequency and in some cases impedes overturning with respect to the undamped case. Secondly, the risk assessment is made developing a multiple stripe analysis to compute univariate fragility curves combining uplift, overturning probability and probability of exceedance. Thirdly, seismic demand hazard curves are obtained for two walls representative of buildings and monumental structures in an Italian site of high seismicity. The PSHA results show the remarkable risk reduction of ultimate limit states, for which the annual exceedance rate is respectively one and two orders of magnitude lower than the undamped case.

Keywords: rocking; seismic control; damped wall; fragility curve; seismic demand hazard curve; restrained rocking wall; out-of-plane; nonlinear dynamic analysis; recentering; seismic vulnerability mitigation

1. Introduction

The analysis of existing masonry structures, especially those belonging to the cultural heritage, requires to follow a multi-level procedure [1], [2]. In it, the local analyses play a crucial role; the elements to assess can be considered as rigid blocks rocking out-of-plane (OOP). The seismic performance of rocking blocks is brought under the attention of many researchers for the preservation of both structural (masonry walls, precast r.c. and timber panels)

and non-structural (cabinets, artistic assets, art and decorative objects, statues) elements. The numerous contributions available in the literature start from the pioneering Housner's work [3] which laid the theoretical foundation of the rocking behavior of rigid blocks. Since then, many contributions were offered, studying the transition of phases between rest, rocking, translation-jump, rotation-jump and sliding phenomena, besides overturning criteria [4]–[6], also using nonlinear static analyses [7], [8]. Rocking as seismic isolation technique was recently proposed considering the capacity of slender structures that survived over the centuries under earthquakes [9]. This concept merges into the *damage avoidance design* intended to realize integrated low damage systems [10]. The idea is to couple recentering systems to hysteretic or viscoelastic dissipators, which should be cost-efficient and replaceable. Indeed, the structure can be seen as composed by rigid rocking blocks or elements with sacrificial devices meant to be damaged under design earthquakes, as "weakest links of the chain" [11]. This way, repair and downtime costs are minimized, as the replacement of specific components, whose access is eased to facilitate inspections, is much simpler and less demanding than the retrofitting of plasticized or broken structural components.

The coupling of dissipative devices to self-centering components or tendons produces a hybrid system associated to a flag-shape force-displacement relationship. The viscous-elastic damper can be located at a certain height from the wall base with the purpose of mitigating its seismic vulnerability. A similar passive seismic device was recently patented and illustrated in [12]. Analytical and numerical approaches were provided to investigate the uplift of anchored rigid blocks [13], [14] and the seismic fragility of furniture, electric or mechanical equipment anchored at the base [15], [16]. When the seismic performance of rocking structures is considered in a probabilistic sense, specific intensity measures must be assumed, as illustrated in [17] for controlled rocking steel braced frame system and a rocking spine system for reinforced concrete infill frames and in [18] for rocking podium structures. Diverse probabilistic models are available in the literature to predict the stochastic behavior of rocking blocks, either free from restraints or restrained. For example, Bakhtiary and Gardoni [19] proposed a probabilistic model to predict the response of rigid symmetric bodies with a Bayesian updating approach. Contento et al. [20] developed a probabilistic model to assess the seismic safety of rigid block-like elements with base isolation and or pendulum mass dampers. This paper has the purpose of investigating the effects of viscous dampers (or dashpots) coupled

with recentering components in masonry walls rocking OOP. The paper is structured such as the risk assessment is performed after a proper selection of ground motions and a preliminary deterministic analysis to discuss the effect of dampers on the transient response. The seismic risk assessment consists in two phases: the determination of univariate fragility curves and the computation of seismic demand hazard curves, to understand the level of improvement in terms of annual exceedance rate is gained with the adopted passive seismic control device. More in detail, Section 2 contains the analytical formulation of the rocking block restrained by a horizontal fluid viscous damper and recentering component. Section 3 illustrates the assumptions of the numerical simulations and the probabilistic models, whereas Section 4 discusses the fragility curves found for slender walls of different size. Section 5 is devoted to the risk assessment through seismic demand hazard curves and compares them in the damped and undamped systems, to quantify the beneficial effect of the seismic control device.

2. Analytical background

This Section contains the analytical background necessary to perform non-linear transient rocking analyses, aimed at discussing the effect of a dashpot and a recentering element.

2.1 General assumptions

The OOP rocking motion of rigid blocks free to rock or horizontally/vertically restrained is studied under the following assumptions: the seismic excitation only acts along a horizontal axis, the foundation on which the block rocks is infinitely stiff, bouncing, sliding and interaction between in-plane and out-of-plane behavior are neglected. The last hypothesis is always valid for enough slender blocks with h/b greater than 4 [21], which is the case of the walls investigated in this paper. Moreover, energy is dissipated during impacts on the corners and – only in the restrained configurations – when the relative velocity of the dashpots is non-zero. Dashpots are considered as linear fluid viscous dampers. The horizontal elastic restraint is assumed to act only up to its own yielding value; once this threshold has been reached, it becomes inactive.

2.2 Equations of motion

The equations of motion of a block purely rocking around its base corners can be obtained through the Euler-Lagrange's formulation. The block is geometrically defined by its size R and its slenderness ratio α, arctangent of height to thickness ratio (Figure 1a). The block can be either free-standing or connected to a fixed support via vertical or horizontal dissipative restraints, in which elastic and/or viscous forces may develop.

For a rectangular block of mass m and inertia moment I_0 (Figure 1b) connected to a damper of equivalent viscous coefficient c installed at a certain height from the base hinge, the equation of motion reads:

$$I_0\ddot{\vartheta} + sgn(\vartheta)mgR\sin[\alpha - sign\,(\vartheta)\vartheta] + \\ +sgn(\vartheta)\,K\beta^2R^2\cos[\alpha - sign\,(\vartheta)\vartheta]\;[\sin\alpha_r - \sin[\alpha - sign\,(\vartheta)\vartheta]] + c\,\beta_d^2R^2\,cos^2\,A_{d,\vartheta}\;\dot{\vartheta} \\ = m\,\ddot{u}_gR\,cos\,A_\vartheta \tag{1}$$

g is the gravity acceleration and K the stiffness of the horizontal restraint, whereas α_r is the angle between the radius vector R_d and the external wall profile, as shown in Figure 1a. The position of the horizontal restraint is defined by $R_d = \beta R$, being β a scalar coefficient variable from 0 (no restraint) to 2 (restraint at the top corner). whenThe term depending on K is calculated as explained in [22]. Similarly, through the Euler-Lagrange's formulation, the term depending on c is obtained [23]. The arguments of the sinusoidal functions are expressed as:

$$A_\theta = \alpha - sgn(\vartheta)\cdot\vartheta;\; A_{r,\vartheta} = \alpha_r - sgn(\vartheta)\cdot\vartheta;\; A_{d,\vartheta} = \alpha_d - sgn(\vartheta)\cdot\vartheta \tag{2}$$

The equation for the free-standing system is obtained from Eq. (1) with the condition $K = c = 0$. The transition from the equation valid for restrained blocks to that coherent for free-standing blocks is considered with a fracture function proposed in [14]:

$$f(\vartheta) = 1 \text{ when } \vartheta(t) > \vartheta_y \\ f(\vartheta) = 0 \text{ when } \vartheta(t) \le \vartheta_y \tag{3}$$

where ϑ_y is the block rotation corresponding to the yielding of the horizontal restraint, which can be fixed according to the used material.

Generally, the displacement time-history is expressed in normalized terms as ϑ/α [24]. In case of statistical analysis, the corresponding engineering demand parameter (EDP) for each realization is the maximum ϑ/α registered over the individual earthquake time. This EDP is that normally selected when the motion is pure rocking since the block returns, if stable, to its original position virtually without any permanent deformation or damage.

(a) (b) (c)

Figure 1 (a) Schematics of the rocking block restrained by a viscous damper coupled with horizontal recentering component; example of rocking control device (LICORD) embedded in a masonry wall (b) with its components (c) (for more details about experimental tests on LICORD refer to [12]**).**

3. Stochastic vulnerability analysis

This Section discusses the fragilities associated to OOP rocking walls strengthened by dampers and recentering components. The purpose is to assess the vulnerability of masonry walls under diverse intensity earthquakes and its reduction thanks to anti-seismic devices functioning as viscous dampers with recentering component [12].

3.1 Methodology

In this paper, the beneficial effect of the damping control device is demonstrated through a methodology applied to two walls of representative geometry. The effect of dampers is investigated through a stochastic analysis applied to slender masonry walls rocking OOP. Non-linear dynamic analyses are performed by solving Eq. (1) with a code developed in MATLAB, and the maximum rotations of rocking walls subject to selected ground excitations are measured. All the analyses are performed assuming a coefficient of restitution function of the slenderness ratio $e = 1 - \frac{3}{2}\sin^2\alpha$ [3]. From the results of the dynamic analyses, the conditional probability that an engineering

demand parameter (EDP or the normalized rotation) overcomes a capacity limit is calculated, given an intensity measure associated to the input action. Afterwards, that probability of exceedance is combined with the uplift and the overturning probability to get the final failure probability (as explained more in detail in Section 3.2).

The two walls are assumed as rectangular blocks representative of typical structural elements in existing masonry buildings: a "building" type wall and a "monumental" type wall (Table 1). The "building" block has dimensions (height x width x thickness) 2.70 m x1.52 m x 0.25 m, with a specific weight of 19 kN/m^3; the consequent mass and geometric properties can be easily calculated and are reported in Table 1. The monumental wall is selected to have the same slenderness ratio ($\boldsymbol{\alpha}$ =0.09, or height/thickness≅11) as the building type wall, dimensions 10.8 m x6.08 m x1.00 m, with a specific weight of 19 kN/m^3. The monumental wall width, which is representative of church façades, has been chosen with the same height-to-width ratio as the building type wall (2.70/1.52=10.6/6.08≅1.8). Walls of other slenderness ratios are not investigated as the slenderness chosen is quite high and therefore the results represent an upper bound of safety assessment.

Both walls rotate out-of-plane (OOP) and the mechanical characteristics of the viscous dampers are calculated considering values reported in [12] for similar devices. In particular, the lower bound of damping coefficient c =1 kNs/m is assumed for the building type wall. That of the monumental wall is assumed to be proportional to its own mass, which is 65.2 times that of the building type wall. The recentering component has stiffness of 10 kN/m for the building wall and 652 kN/m for the monumental wall.

Table 1 Geometric and mechanical parameters of the analyzed blocks and limit states for fragilities. Errore. L'origine riferimento non è stata trovata.

wall	mass [kg]	Slenderness ratio $\boldsymbol{\alpha}$ [-]	Radius vector R [m]	c [kN/m/s]	K [kN/m]
"building"	1960	0.09	1.36	0-1	0-10
"monumental"	127850	0.09	5.42	0-65.2	0-652
Limit states	LS0-rocking initiation or uplift	LS1-limited rocking	LS2-moderate rocking	LS3-static threshold	LS4-near-collapse
$EDP_{lim} = \frac{\vartheta_{max}}{\alpha}$	0.0	0.1	0.4	1.0	1.5

The five limit states (LS) considered in the stochastic analyses are rocking initiation, limited rocking, moderate rocking, static threshold and near-collapse rocking. Each LS is identified by an $EDP = \frac{\vartheta_{max}}{\alpha}$ [25] as shown in Table 1. The rocking initiation $LS0$ corresponds to the uplift condition or $\vartheta \neq 0$. Uplift occurs when the peak ground acceleration is greater than the minimum ground acceleration, $\ddot{u}_{g,min} = \tan\alpha$. The numerical value to set in the MATLAB code for rocking initiation is set to 1E-4. The *limited rocking* $LS1$ corresponds to $\frac{\vartheta_{max}}{\alpha} = 0.1$ and it was considered by Dimitrakopoulos et al. [25] as a promising balance of the benefits of rocking isolation, excluding risk of overturning. The *moderate rocking* $LS2$, the static threshold $LS3$ and the *near-collapse* $LS4$ correspond to $\frac{\vartheta_{max}}{\alpha} = 0.4$, 1.0 and 1.5 respectively. The static threshold limit state $LS3$ refers to the limit condition of static safety, that is $\vartheta = \alpha$. $LS1$ can be seen as serviceability LS, whereas $LS2$, $LS3$ and $LS4$ as ultimate LS.

3.2 Fragility analysis

The fragility curves (FCs) are obtained by post-processing the results of the non-linear seismic analyses, considering only demand uncertainties. These realizations are treated by calculating fragility as conditional probability of failure, where the demand is represented by the $EDPs$ calculated from transient analyses and the capacity C is defined by the LS described in the previous section. The $EDPs$ clearly depend on the seismic input, in turn defined by specific intensity measures (IMs). The conditional probability of exceedance is expressed by the standard cumulative distribution function Φ assuming a lognormal distribution of the rocking cases (excluding overturning cases):

$$P_{ex} = P(EDP > C|IM) = \Phi\left(\frac{\ln D - \ln C}{\beta_{D|IM}}\right). \quad (4)$$

$\beta_{D|IM}$ is the logarithmic standard deviation, or dispersion, of the demand conditioned on the IM level. D is the median structural demand (= EDP) described by a power law in case of univariate FCs:

$$D = a\, IM^b. \quad (5)$$

Once D is calculated, Equation (4) applies to find the conditional probability of exceedance . Considering only the exceedance probability P_{ex} to stochastically assess the safety of the rocking block would bring to wrong estimations, because P_{ex} neglects the overturning cases for which a two-level categorical probability must be computed. Consequently, the correct probability $P_{EDP|IM}(edp|im_y)$ that $EDP > edp$ given $IM = im$ is computed also taking into account the probability of uplift P_{UP} and the probability of overturning P_{RO}. The latter are calculated by means of the method of maximum likelihood [26] which allows the estimation of the fragility function parameters (mean $\hat{\mu}_{RO}$ and standard deviation $\hat{\beta}_{RO}$) assuming that the IM values of the ground motions causing uplift/overturning are lognormally distributed and that the uplift/overturning occurrence follows a binomial distribution. The three probabilities are then combined to obtain the failure probability as follows [27]:

$$P_{EDP|IM}(edp|im_y) = P_{UP}[P_{RO} + (1 - P_{RO})P_{ex}] \quad (6)$$

The intensity measures (IMs) are links between the seismic hazard of the site and the structural response of a building located in that site. Many research contributions are available to assess the ability of specific IMs to provide reliable estimates of rocking structural response as illustrated in [17]. In the present paper, the fragilities are obtained considering as IM the peak ground acceleration (PGA).

For what concerns the computational time, each analysis requires from 12 to 15 hours for each of the six systems (free wall, wall+damper, wall+damper+recentering component, two geometries, considering 80 earthquakes and 6 intensity measure levels) with a core i7 8th gen CPU and 8GB RAM. The time step is not fixed but automatically varied by the MATLAB's ODE 45 solver [28].

3.3 Selection of seismic records

A robust probabilistic analysis requires the selection of significant ground motions, which should capture the intensities, return periods, duration and frequency contents of the possible seismic events for diverse civil engineering systems [29]. The selection process is similar to that adopted by Tabandeh & Gardoni [30] and by Huang et al [31]. The ground motions are selected such as that their response spectra are spectrum compatible. The 5% damping spectrum is obtained for the Italian site L'Aquila (long. 13.3944°, lat. 42.366°), assuming site

class A, topographic category T1, return period 475 years [32]. The matching process is performed by the software package REXEL [33] imposing a lower tolerance by 10% and an upper tolerance by 30% as recommended in [32]. The compatibility period range is included between 0.15 seconds and 2 seconds.

All the earthquakes are collected from the Engineering Strong Motion database (ESM [34]). The ground motion prediction equation (GMPE) is that proposed by Ambraseys et al. [35], fitted on records with magnitude M_W from 4.0 to 7.5 and source-distance R up to 200 km.

The following bins are considered:

- BIN SMSR (small M and small R): $5.5 \leq M_W \leq 6.5$ and $15 \leq R \leq 30$ km
- BIN SMLR (small M and large R): $5.5 \leq M_W \leq 6.5$ and $30 \leq R \leq 50$ km

The preliminary inventory of the BIN SMSR consists of 24 events with 94 records among which the spectrum compatibility is found imposing a maximum mean amplification factor by 2. The preliminary inventory of the BIN SMLR consists of 23 events with 72 records among which the spectrum compatibility is found imposing a maximum mean amplification factor by 5. Twenty combinations of seven seismic records each are extrapolated (Figure 2a); then, each bin is formed with twenty earthquakes with consistent characteristics and belonging to different distinct events. The number of records in the two bins is the same to provide an even representation of the possible characteristics without introducing bias into the assessment of the seismic demand variables [31]. The structural analyses are performed for both bins doubling the number of earthquakes, considering positive and negative signs of the shocks, for a total number of eighty analyses for each IM level.

Especially for existing masonry buildings, local OOP failure modes are likely to occur in the upper floors, where the stabilizing effect of gravitational loads is lower and the connection with roof is often deficient. For this reason, these seismic inputs should be magnified considering the dynamic amplification that walls experience whether their rotational hinge is at a certain height from the foundation. To account for this phenomenon and assuming a physically reliable value and in favour of safety, an amplification factor of 2 is assumed in the structural analyses for all the earthquakes. The results are therefore conditioned to this assumption.

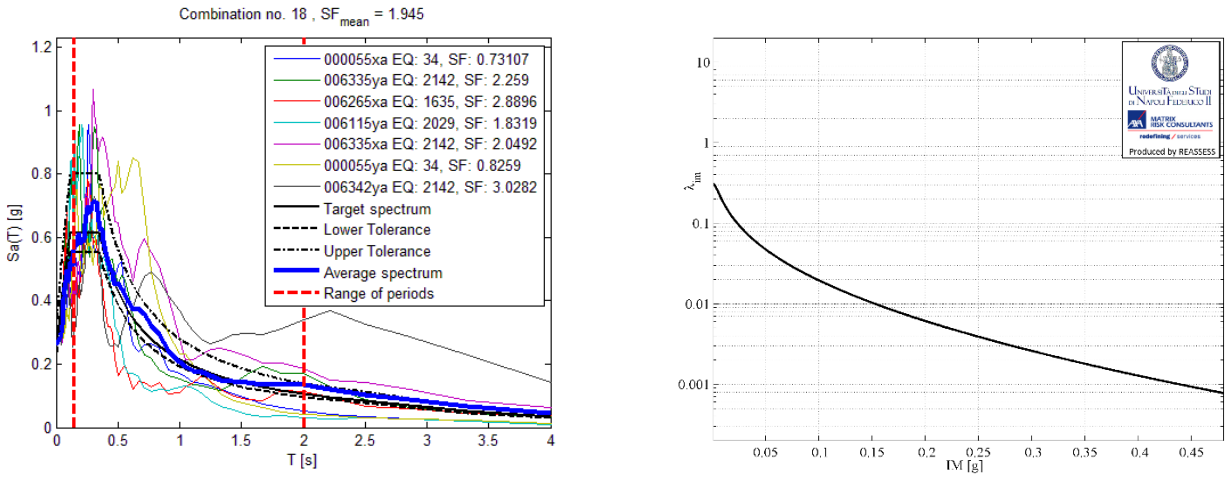

(a) (b)

Figure 2 Selection of ground motions and hazard parameters: (a) example of combination of spectrum-compatible natural records from REXEL [33]**; (b) annual exceedance rate of IM=PGA for the reference site (L'Aquila) computed from a PSHA with REASSESS** [36]**.**

3.4 PSHA: methodology to compute seismic demand hazard curves

In this section a probabilistic approach applicable to free and damped rocking masonry walls is presented. A similar probabilistic method, which was recently applied to walls restrained by elasto-plastic tie-rods in [27], was proposed in [37]. Here, three systems are considered: free-standing wall, wall restrained by a top damper, wall restrained by a top damper with recentering element (Figure 1). Analogously to the fragility analysis, the EDP is the maximum normalized amplitude rotation ϑ/α of the response time history. A MSA is performed because it is independent on the conditioning IM, in contrast to the limitations of the intensity-based assessment. In the latter, indeed, the distribution $f_{EDP|IM}(edp|im_y)$ for different IMs (e.g. PGA, PGV or PGD) having the same annual exceedance rate $\lambda_{IM}(im_y) = y$ can be different [37]. The procedure followed in the analysis is thoroughly illustrated in [27] and here briefly recalled.

Firstly, a representative ensemble of n ground motions is selected (in our case $n = 80$, Section 3.3). Then, the seismic hazard curve (Figure 2b) is obtained as relationship of the annual exceedance rate λ_{IM} with m values (in this case $m = 6$) of the selected intensity measure PGA.

The PSHA is performed through the open-source code REASSESS [36] for the same site used in the selection of ground motions (Section 3.3), L'Aquila, obtaining the relationship between annual exceedance rate and reference intensity measure, PGA. This curve is necessary for computing the seismic demand hazard curves; the annual exceedance rate curve is drawn for six levels of IM, from IM1=0.10g to IM6=0.56g (Table 2), the same used in the MSA to obtain the fragility curves. Each of the IM levels corresponds to specific return periods reported in the same table.

Afterwards, n rocking analyses are performed for each i^{th} IM level ($i = 1, \dots, m$), collecting the individual realizations to be elaborated, although the scaling of the record is not strictly necessary when MSA is performed. Finally, the annual exceedance rates of the EDP, which represent the ordinates of the seismic demand hazard curve (SDHC) are computed with the following integral [37]:

$$\lambda_{EDP}(edp) = \int_0^{\infty} P_{EDP|IM}\left(edp\middle|im_y\right)\left|\frac{d\lambda_{IM}(im)}{dIM}\right|dIM \quad (7)$$

$P_{EDP|IM}\left(edp\middle|im_y\right)$ is computed with Eq. (6), whilst the derivative $\frac{d\lambda_{IM}(im)}{dIM}$ is calculated from the hazard curve. It is worth noting that the first and the last values of return period in Table 2 are solely used for calculating the derivative $\frac{d\lambda_{IM}(im)}{dIM}$ used in Eq. (7), and therefore the corresponding IM do not need to be explicated.

Table 2 Values of peak ground acceleration and corresponding return periods of the seismic hazard curve computed from a PSHA with REASSESS [36].

PGA	-	IM1=0.100g	IM2=0.190g	IM3=0.220g	IM4=0.328g	IM5=0.448g	IM6=0.559g	-
Return period (years)	30	50	150	201	475	804	979	2004

The SDHC so obtained are relevant for a risk assessment of rocking walls since hazard and vulnerability are considered together. These curves are therefore used to compare the performance of undamped and damped rocking walls, to understand the beneficial effect offered by springs and dampers in stochastic terms.

4. Fragility curves from MSA

For all the seismic inputs and for all the scaled intensity measures, the addition of the dissipative restraint mitigates the rotation amplitude, as shown in Figure 3 for some selected rotation time-histories. In general, the damper alone (violet curve) reduces the normalized rotation peaks or delays overturning with respect to the free-standing wall without restraint (red curve), whereas the coupling of it with a spring (black curve) further attenuates the motion (Figure 3a), increases the rotation frequency (Figure 3a and Figure 3c) and impedes overturning (Figure 3b).

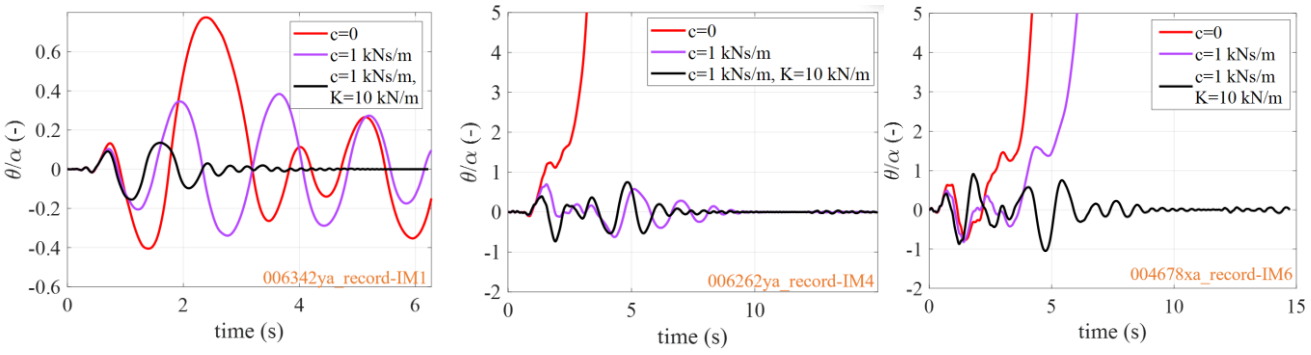

(a) (b) (c)

Figure 3 Time-history analysis results for selected earthquakes (the characteristics, record stations and dates of the earthquakes can be found in [33]).

The univariate fragility curves are calculated from the EDPs (plotted against the intensity measures PGA and PGV in Figure 4a, d for the building type wall) to assess the mitigation of seismic vulnerability due to the damper with the methods illustrated in Section 3.2. The limit states LS1 (limited rocking), LS2 (moderate rocking), LS3 (static threshold) and LS4 (near-collapse rocking), listed in Table 1 are considered. The graphs reported in Figure 4a-c refer to the whole set of seismic records, whereas Figure 4d-f show the results only for BIN SMSR (Section 3.3). The formers are more reliable, although the two sets of curves are very similar each other, demonstrating that the selection of ground motion is valid. Figure 4b reports the probability of overturning for the set BIN SMSR+SMLR whilst the probability of exceedance for each LS is shown in Figure 4e for BIN SMSR. It should be noticed that the probability of exceedance does not represent the overcoming of a limit state, but the overcoming of a limit state conditioned on the occurrence of the block not overturning. Thus, these curves can be considered as a simple tool to compare the fragilities in case of different damper properties or boundary conditions, but they do not

provide the actual failure probability (which is instead calculated with Eq. (6) and reported in Figure 4c and Figure 4f).

As expected, the overturning probability increases with the IM amplitude for each system. Such an increase is particularly evident for the rocking wall without anti-seismic devices, whilst it is basically null or assume very low values for the case of block with damper. If the wall is also horizontally restrained by a recentering element of stiffness K, the overturning probability is even lower but only for seismic intensity over PGA=0.9g (Figure 4b).

Thus, in general the addition of the dashpot (damper with damping coefficient c) strongly reduces the seismic vulnerability of the wall, as demonstrated by the failure probability curves (Figure 4c for the whole set of ground motions, and Figure 4f for BIN SMSR). The recentering element (spring of stiffness K) implies a further but slight reduction of failure probability up to 1g PGA earthquakes (Figure 4c, Figure 4f), due to its already mentioned beneficial effects. For higher intensity earthquakes, the elastic component is sensitively more beneficial than the damper alone. The quantitative variation of safety assessment can be computed by analyzing Figure 4c, valid for the building type wall, which is more seismically vulnerable than the monumental type wall due to the scale effect highlighted in [3]:

1. An equivalent damping coefficient of $c = 1\frac{kNs}{m}$ implies remarkable reductions of the OOP vulnerability of the wall. This value is half of that used for a passive seismic control device presented in the literature to control rocking of masonry walls (Table 1 in [12]). Therefore, even a low damping coefficient is favourable for reducing the seismic vulnerability of the wall;

2. The maximum reduction of failure probability between damped (without spring) and undamped wall in case of high-intensity earthquakes is obtained for the near-collapse limit state (LS4), with a percentage of 81% at a value of $IM = PGA = 1.05g$. This behavior is expected since for high IMs the wall dynamic amplitude is greater, and the damping effect is more relevant for ultimate limit states;

3. The maximum reduction of failure probability in case of low/moderate intensity earthquakes is registered for the serviceability limit state (LS1), obtaining a reduction percentage by 66% at a value of $IM = PGA = 0.2g$;

4. The maximum difference of failure probability between wall + damper and wall+damper+spring is less than 10% and becomes greater for high-intensity ground motions and ultimate limit states. This occurs because the recentering effect plays a role for high-intensity earthquakes smoothening the response peaks. A much remarkable difference is observed for LS4, with half failure probability in case of spring, since the latter, although in a few cases, impedes the wall to overturn (see also Figure 3c).

BIN SMSR + SMLR

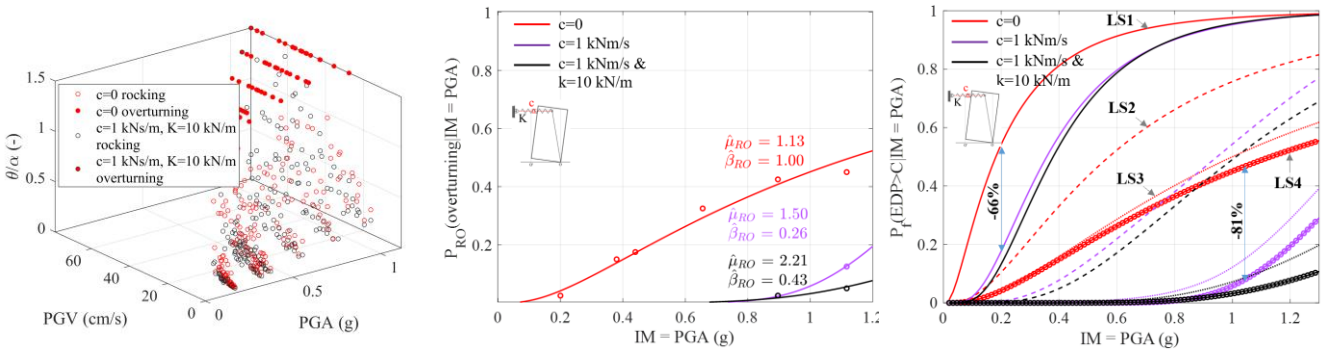

(a) (b) (c)

BIN SMSR

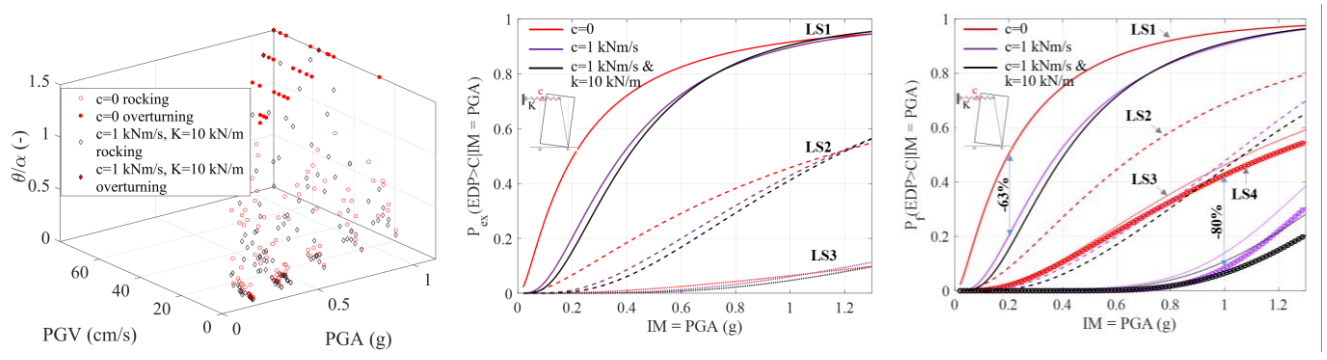

(d) (e) (f)

Figure 4 Fragility curves from MSA: (a, d) EDPs; (b) probability of exceedance (Eq. (4)); (e) probability of overturning; (c, f) failure probability (Eq. (6)).

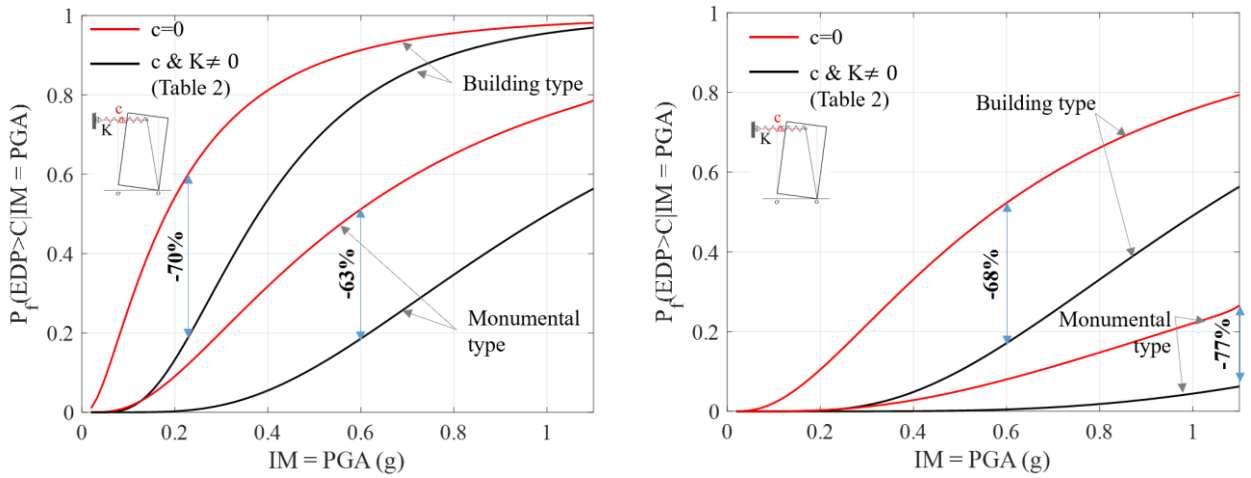

Figure 5 Comparison of fragility curves for masonry walls of same slenderness and different size: (a) limited rocking limit state LS1; (b) moderate rocking limit state LS2.

The comparison of failure fragility curves obtained for the building type wall and the monumental wall allows making additional remarks (Figure 5). First of all, as already mentioned, the failure probability is lower for the monumental wall as the block of same slenderness but with greater size is more stable. There is not a specific trend for the minor or major beneficial effect due to the damper considering either the building type wall or the monumental wall. The percentage reduction of fragility is more or less similar for the limited rocking limit state (Figure 5a) and for the moderate rocking limit state (Figure 5b), being of the order of 60%-80%. The monumental type wall even without seismic control device has a very low fragility, being slightly more than 20% for rare 1.2g PGA earthquakes considering the moderate limit state, where the limit normalized rotation is 0.4. For higher limit states, the fragility of the free-standing monumental wall is even lower and therefore not reported.

5. Risk analysis and seismic demand hazard curves

The seismic demand hazard curves plot the annual exceedance rate in terms of annual exceedance rate (Figure 6a) and of return periods (inverse of annual exceedance rate, Figure 6b). The circles of the SDHC are each representative of the five limit states reported in Table 1, from the uplift to the near-collapse limit state. From the observation of the SDHC it is evident the great improvement achieved by controlling rocking motion through a

damper. A further reduction of seismic risk is visible for the system with the recentering element, particularly for the three ultimate limit states of static, moderate and near-collapse rocking.

In particular, the following considerations can be drawn from Figure 6:

1. the risk associated to the uplift limit state does not vary with the type of system (restrained or free). Indeed, for free-standing and damped wall the return period is always 39 years. This is due to the fact that damper and spring are mobilized only for non-null rotations, as spring is not pre-compressed and the initial input velocity is zero;

2. the annual frequency of exceedance rate for the limited rocking limit state decreases by 42% passing from the undamped to damped case; the further decrease recorded in case of the additional spring component is negligible, being less than 6%;

3. The moderate rocking limit state implies a more evident beneficial effect of the damper, for which the return period increases by at least 2.5 times with respect to the wall without restraints;

4. regarding the exceedance of the static threshold limit state, this event is exceeded once in 265 years for the freestanding block, in 2721 and 4576 years respectively for the simply damped wall and that with damper and spring. Such a remarkable effect, which reduces by at least one order of magnitude the annual exceedance rate, reveals the great enhancement achieved for ultimate limit states.

5. Such a decrease is even more evident for the near-collapse limit state arbitrarily fixed at a normalized rotation of 1.5, being the annual frequency rate of the damped cases of two orders of magnitude lower than the undamped case. For both ultimate limit states LSstatic and near-collapse LS the addition of the recentering component almost doubles the return period for which the event occurs.

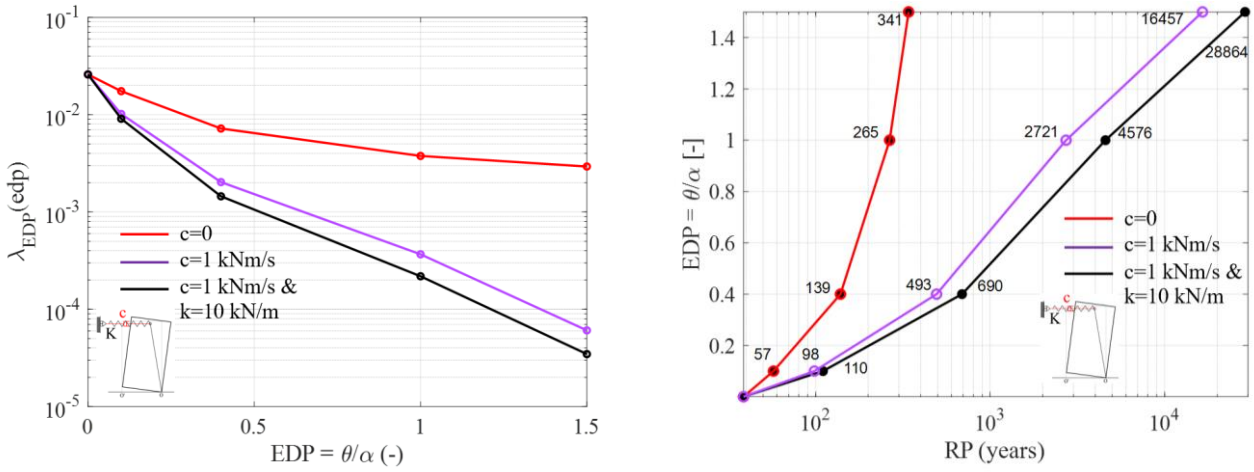

(a) (b)

Figure 6 Seismic demand hazard curves in terms of (a) annual exceedance rate and (b) return period from Eq. (7).

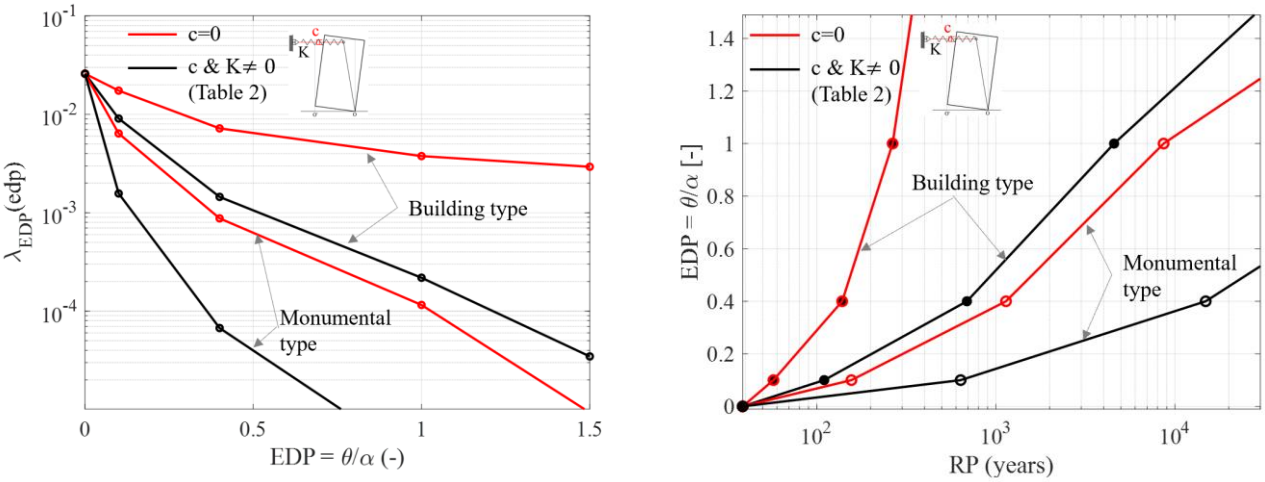

(a) (b)

Figure 7 Comparison of seismic demand hazard curves of building type and monumental type walls in terms of (a) annual exceedance rate and (b) return period from Eq. (7).

A last comparison is performed between building type and monumental type walls in Figure 7. The building type wall restrained by viscous damper and spring (top black curve in Figure 7a) has a slightly greater annual exceedance rate than that of the monumental type wall without damper (red curve at the bottom in Figure 7a). In any case, the reduction of risk is more remarkable for the ultimate limit states, in particular for the static threshold and the near-collapse limit states.

These beneficial effects confirm that limiting OOP modes with passive seismic control devices is a key aspect for the seismic vulnerability mitigation of existing masonry buildings. The added value of the damper as innovative device [12] consists in the possibility of controlling OOP modes reducing the number and amplitude of oscillations and consequently limiting the risk of damage to the rocking wall itself and to the adjacent structures (horizontal diaphragms, arches, vaults and sidewalls).

Summarizing, these risk analyses are recommended due to the record-to-record variability typical of rocking analyses performed on restrained masonry walls. Moreover, the comparison between SDHC is a straightforward and useful tool to quantify the level of improvement reached with seismic control devices. Such a comparison can be used for a specific design case or to build abaci to estimate the increase of safety level gained by diverse passive seismic control systems.

Conclusions

This paper presented the results of stochastic analyses to assess the mitigation of seismic risk of damped rocking blocks. Examining the structural analysis results, it is observed that the damper reduces the dynamic response or delays overturning with respect to the free-standing wall without restraint, whereas the coupling of it with a spring further attenuates the motion, increases the rotation frequency and impedes overturning.

These beneficial effects are also observed in stochastic analysis, as demonstrated by the failure probability curves. Even dampers with low damping coefficients (of the order of $c = 1\frac{kNs}{m}$) cause remarkable reductions of the OOP vulnerability of the building type wall, which is the most vulnerable. The additional recentering element (with stiffness of K=10 kN/m for a wall mass of about 2 tons) implies a further but slight reduction of failure probability up to 1g PGA earthquakes, whereas for higher intensity earthquakes, the elastic component is sensitively more beneficial than the damper alone. The maximum reduction of failure probability between damped (without spring) and undamped wall in case of high-intensity earthquakes is obtained for the near-collapse limit state, with a percentage of 81% at a value of $PGA = 1.05g$. The maximum reduction of failure probability in case of low/moderate intensity earthquakes is registered for the serviceability limited rocking limit state, obtaining a reduction percentage by 66% at a value of $PGA = 0.2g$. The failure probability is lower for the monumental wall

as the block of same slenderness but with greater size is more stable. There is not a specific trend for the minor or major beneficial effect due to the damper considering either the building type wall or the monumental walls but it is comparable, being of the order of 60%-80% for all the limit states. Therefore, the seismic behavior enhancement is clear with the use of this seismic control device. For what concerns the risk analysis, seismic demand hazard curves (SDHC) proved to be an effective tool to quantify the level of improvement achieved by controlling the rocking response through damper and springs. The numerical analysis showed that the most positive effects are obtained for ultimate limit states. Indeed, in the moderate rocking limit state, there is a minimum increase of the occurrence return period by at least 2.5 times with respect to the undamped wall. For the static threshold and near-collapse limit states, the annual exceedance rate is one and two orders of magnitude lower than the undamped case respectively.

These beneficial effects confirm the relevance of limiting OOP modes with passive seismic control devices in the vulnerability mitigation of existing masonry buildings. With specifically design of damping and stiffness properties of these devices through SDHC, OOP rocking can be controlled by reducing the number and amplitude of oscillations and consequently limiting the level of damage to the rocking wall itself and to the adjacent structures (horizontal diaphragms, arches, vaults and sidewalls).

References

[1] C. Casapulla, L. U. Argiento, and A. Maione, Seismic safety assessment of a masonry building according to Italian Guidelines on Cultural Heritage: simplified mechanical-based approach and pushover analysis. *Bulletin of Earthquake Engineering*, **16**, 2809–2837, 2018.

[2] C. Casapulla, A. Maione, and L. U. Argiento, Seismic analysis of an existing masonry building according to the multi-level approach of the italian guidelines on cultural heritage. *Ingegneria Sismica*, **34**, 40–59, 2017.

[3] G. W. Housner, The behavior of inverted pendulum structures during earthquakes. *Bulletin of the Seismological Society of America*, **53**, 403–417, 1963.

[4] I. N. Psycharis and P. C. Jenning, Rocking of slender rigid bodies allowed to uplift. *Earthquake Engineering & Structural Dynamics*, **11**, 57–76, 1983.

[5] I. Caliò and A. Greco, Large displacement behavior of a rocking flexible structure under harmonic excitation. *JVC/Journal of Vibration and Control*, 2016.

[6] C. Casapulla and A. Maione, Free Damped Vibrations of Rocking Rigid Blocks as Uniformly Accelerated Motions. *International Journal of Structural Stability and Dynamics*, **17**, 1–19, 2016.

[7] C. Casapulla, A. Maione, and L. U. Argiento, Performance-based seismic analysis of rocking masonry façades using non-linear kinematics with frictional resistances: a case study. *International Journal of Architectural Heritage*, 2019.

[8] C. Casapulla and A. Maione, Experimental and Analytical Investigation on the Corner Failure in Masonry Buildings: Interaction between Rocking-Sliding and Horizontal Flexure. *International Journal of Architectural Heritage*, 2018.

[9] N. Makris, A half-century of rocking isolation. *Earthquakes and Structures*, **7**, 1187–1221, 2014.

[10] A. J. J., P. Gokhan, and M. J. B., Rocking Wall–Frame Structures with Supplemental Tendon Systems. *Journal of Structural Engineering*, **130**, 895–903, 2004.

[11] S. Pampanin, Towards the ``Ultimate Earthquake-Proof'' Building: Development of an Integrated Low-Damage System. , in *Perspectives on European Earthquake Engineering and Seismology: Volume 2*, A. Ansal, Ed. Springer International Publishing, 2015, 321–358, .

[12] L. Giresini, F. Solarino, F. Taddei, and G. Mueller, Experimental estimation of energy dissipation in rocking masonry walls restrained by an innovative seismic dissipator (LICORD). *Bulletin of Earthquake Engineering*, **19**, 2265–2289, 2021.

[13] N. Makris and M. F. Vassiliou, Dynamics of the Rocking Frame with Vertical Restrainers. *Journal of Structural Engineering*, **141**, 2015.

[14] N. Makris and C. J. Black, Uplifting and Overturning of Equipment Anchored to a Base Foundation. *Earthquake Spectra*, **18**, 631–661, 2002.

[15] S. W. Swan and R. Kassawara, The use of earthquake experiences data for estimates of the seismic fragility of standard industrial equipment. , in *ATC 29-1 Proc of Seminar on Seismic Design, Retrofit and Performance of Nonstructural Components, Applied Technology Council*, 1998, 313–322, .

[16] G. Cremen and J. W. Baker, Improving FEMA P-58 non-structural component fragility functions and loss predictions. *Bulletin of Earthquake Engineering*, **17**, 1941–1960, 2019.

[17] M. Shokrabadi and H. V Burton, Ground Motion Intensity Measures for Rocking Building Systems. *Earthquake Spectra*, **33**, 1533–1554, 2017.

[18] K. E. Bantilas, I. E. Kavvadias, L. K. Vasiliadis, and A. Elenas, Seismic fragility and intensity measure investigation for rocking podium structures under synthetic pulse-like excitations. *Earthquake Engineering & Structural Dynamics*, **50**, 3441–3459, 2021.

[19] E. Bakhtiary and P. Gardoni, Probabilistic seismic demand model and fragility estimates for rocking symmetric blocks. *Engineering Structures*, **114**, 25–34, 2016.

[20] A. Contento, P. Gardoni, A. Di Egidio, and A. de Leo, Probabilistic Models to Assess the Seismic Safety of Rigid Block-Like Elements and the Effectiveness of Two Safety Devices. *Journal of Structural Engineering*, **145**, 4019133, 2019.

[21] P. R. Lipscombe and S. Pellegrino, Free rocking of prismatic blocks. *Journal of Structural Engineering*, **119**, 1387–1410, 1993.

[22] L. Giresini and M. Sassu, Horizontally restrained rocking blocks: evaluation of the role of boundary conditions with static and dynamic approaches. *Bulletin of Earthquake Engineering*, **15**, 385–410, 2017.

[23] L. Giresini, F. Taddei, F. Solarino, G. Mueller, and P. Croce, Influence of stiffness and damping parameters of passive seismic control devices in one-sided rocking of masonry walls. *Journal of Structural*

Engineering (ASCE), 2021.

[24] S. Colonna, S. Imperatore, and B. Ferracuti, Fragility curves of masonry church façades. , in *COMPDYN 2019 7th ECCOMAS Thematic Conference on Computational Methods in Structural Dynamics and Earthquake Engineering M. Papadrakakis, M. Fragiadakis (eds.) Crete, Greece, 24–26 June 2019*, 2019.

[25] E. G. Dimitrakopoulos and T. S. Paraskeva, Dimensionless fragility curves for rocking response to near-fault excitations. *Earthquake Engineering & Structural Dynamics*, **44**, 2015–2033, 2015.

[26] J. W. Baker, Efficient analytical fragility function fitting using dynamic structural analysis. *Earthquake Spectra*, **31**, 579–599, 2015.

[27] F. Solarino and L. Giresini, Fragility curves and seismic demand hazard analysis of rocking walls restrained with elasto-plastic ties. *Earthquake Engineering & Structural Dynamics*, **50**, 3602–3622, 2021.

[28] MATLAB. v9.8.0.1359463 (R2020a) Update 1. The MathWorks Inc., Natick, Massachusetts, 2020. . .

[29] H. Krawinkler, R. Medina, and B. Alavi, Seismic drift and ductility demands and their dependence on ground motions. *Engineering Structures*, **25**, 637–653, 2003.

[30] A. Tabandeh and P. Gardoni, Empirical Bayes Approach for Developing Hierarchical Probabilistic Predictive Models and Its Application to the Seismic Reliability Analysis of FRP-Retrofitted RC Bridges. *ASCE-ASME Journal of Risk and Uncertainty in Engineering Systems, Part A: Civil Engineering*, **1**, 4015002, 2015.

[31] Q. Huang, P. Gardoni, and S. Hurlebaus, Probabilistic Seismic Demand Models and Fragility Estimates for Reinforced Concrete Highway Bridges with One Single-Column Bent. *Journal of Engineering Mechanics*, **136**, 1340–1353, 2010.

[32] Decreto Ministeriale 17/01/2018, Italian Technical Standards for buildings (Nuove Norme Tecniche per le Costruzioni, in italian). . 2018.

[33] I. Iervolino, C. Galasso, and E. Cosenza, REXEL: Computer aided record selection for code-based seismic

structural analysis. *Bulletin of Earthquake Engineering*, 2010.

[34] L. Luzi, R. Puglia, and E. Russo, Engineering Strong Motion database (ESM), version 1.0, Istituto Nazionale di Geofisica e Vulcanologia, Observatories & Research Facilities for European Seismology-Orfeus Working Group 5. . 2016.

[35] N. N. Ambraseys, K. A. Simpson, and J. J. Bommer, Prediction of Horizontal Response Spectra in Europe. *Earthquake Engineering & Structural Dynamics*, **25**, 371–400, 1996.

[36] E. Chioccarelli, P. Cito, I. Iervolino, and M. Giorgio, REASSESS V2.0: software for single- and multi-site probabilistic seismic hazard analysis. *Bulletin of Earthquake Engineering*, **17**, 1769–1793, 2019.

[37] B. A. Bradley, A comparison of intensity-based demand distributions and the seismic demand hazard for seismic performance assessment. *Earthquake Engineering & Structural Dynamics*, **42**, 2235–2253, 2013.